Fabrication of Multiphase Liquid Metal Composites

Containing Gas and Solid Fillers: from Pastes to Foams

Shreyas Kanetkar,¹ Najam Ul H. Shah,¹ Rohit M. Gandhi,¹ Aastha Uppal,² Michael D. Dickey,³ Robert Y. Wang,^{1*} and Konrad Rykaczewski^{1,4*}

1. School for Engineering of Matter, Transport and Energy, Arizona State University

Tempe, AZ, 85287, United States

- 2. Intel Corporation, 5000 W. Chandler Blvd., Chandler, AZ, 85226, United States
- 3. Department of Chemical and Biomolecular Engineering, North Carolina State University,

Raleigh, North Carolina 27695, United States

4. Julie Ann Wrigley Global Futures Laboratory, Arizona State University, Tempe, Arizona

85287, United States

Abstract: Gallium-based liquid metals (LMs) are suitable for many potential applications due to their unique combination of metallic and liquid properties. However, due to their high surface tension and low viscosity, LMs are challenging to apply to substrates in useful shapes such as dots, wires, and films. These issues are mitigated by mixing the LMs in air with other materials, such as mixing with solid particles to form LM-solid pastes or mixing with gases to form LM foams. Underlying these deceivingly simple mixing processes are complex and highly intertwined microscale mechanisms. Air micro-bubbles are inevitably incorporated while making LM pastes, making them partly foams. On the other hand, for foaming of LM to occur, a critical volume content of solid particles must be internalized first. Consequently, both LM pastes and foams are multiphase composites containing solid and fluid micro-components. Here we systematically study the impact of the mixing procedure, the solid particle size and volume fraction (SiO₂) on the air content of the multiphase LM composites. We demonstrate that decreasing the particle size and increasing their volume fraction substantially decreases the composite density (i.e., increases air entrapment). The foaming process can also be enhanced with the use of high-speed mechanical mixing, albeit leading to the formation of a more disordered internal structure. In contrast, manual mixing with larger micro-particles can promote the formation of more paste-like composites with minimal air content. We explain the microscopic mechanisms underlying these trends by correlating macroscopic measurements with cross-sectional electron microscopy of the internal structure.

Keywords: liquid metal, foams, pastes, silica, gallium

1. Introduction

Gallium-based room-temperature liquid metals (LMs) uniquely combine metallic properties, such as high electrical and thermal conductivity, with those of a liquid. Unlike mercury, LMs are nontoxic and have negligible vapor pressure, and thus safer to use. There are many literature reports demonstrating the application of LMs in integrated circuit thermal management, stretchable electronic devices, medicine, and energy generation thanks to these useful attributes.^{1–} However, LMs have several features that make repeatable deployment challenging.

LMs have a low viscosity and high surface tension, making applying-to and patterning-on various substrates challenging. $^{7-9}$ For example, when dispensed via a syringe on a substrate, LMs tend to bead up into spherical droplets or form unpredictable films rather than making device-relevant shapes such as thin wires or sheets. Additionally, the nearly instantaneous formation of an ≈ 3 nm thick surface oxide causes the metal to flow along the path of least resistance depending on where the oxide ruptures in response to stress. Blending LMs with other materials, including solid and fluid fillers, mitigates many of these issues to various extents and can also enhance many properties (*e.g.*, adding 40% volume fraction of tungsten particles increases the thermal conductivity three-fold.

In principle, the high cohesive energy of liquid metal should make incorporating other materials into them difficult. Interestingly, this is not a problem since the native oxide can fully or partially 'envelope' foreign materials during mixing. ¹¹ As such, many solid fillers have been added to LMs, including copper, ^{12–15} iron, ^{14,16,17} nickel, ^{18–22} silver, ^{21,23,24} magnesium, ²⁵ gadolinium, ²⁶ tungsten, ¹¹ boron nitride, ²⁵ silicon carbide, ²⁷ silicon dioxide (SiO₂), ^{28,29} copper-iron alloy, ³⁰ steel, ¹⁷ diamond, ³¹ graphene, ³² and carbon nanotubes. ^{33,34} Several secondary fluids, including air and silicone oil, have also been incorporated into LMs to create foams ^{35–40} or emulsions. ^{41,42} In almost

all cases, the solid particles are simply mixed into the LM in an air environment. Similarly, foams containing LM and air form naturally when LM is stirred within an air environment.^{35–39}

Underlying these deceivingly simple mixing processes are complex and intertwined microscale mechanisms. We previously showed that when mixing LM with solids, oxide patches form and adhere to individual particles, enabling the internalization of even highly "LM-phobic" particles into the liquid. We speculated that air bubbles are inevitably incorporated during the mixing process of the LM-solid pastes, making them part foam. In turn, we also showed that a critical fraction of solid oxide flakes has to be incorporated from the air-liquid interface before the onset of air bubble internalization into the liquid metal and foam formation. In other words, there are no "pure" LM-particle pastes or LM foams, but multiphase LM composites always contain solid and gas components. By definition, foams should have air pockets. Yet, the presence of air pockets when adding functional solid particles to LM can be undesirable. For example, the electrical or thermal conductivity of the LM composites generally decreases with increasing air content. However, despite the numerous studies on particle addition to LMs, 12-34 the associated foaming has not been addressed.

To this end, we study the impact of the mixing procedure, the solid particle size and volume fraction on air entrapment in the multiphase LM composites. Through density measurements and cross-sectional imaging, we demonstrate several consistent influences of these parameters on the volume fraction and structure of incorporated air pockets. We use our results to infer microscopic mechanisms underlying the observed trends and to provide general guidelines for adjusting the fabrication procedure to create multiphase composites with predominantly paste-like or foam-like characteristics.

2. Results and Discussion

2.1 Illustration of fabrication method impact on the multiphase LM composite structure

To illustrate the impact of the fabrication method on the LM composites, we mixed liquid gallium heated to over 50°C on a hot plate with a 10% volume fraction of 5 µm SiO₂ particles (LM-SiO₂) in four ways that are representative of possible variations in prior literature¹¹⁻³⁴ (see Experimental Section for details). In particular, we mixed the particles with the LM for 20 minutes (no unmixed particles were detected visually after that time in any of the cases) manually 11,15,17,22,26-29 using two different size mortar and pestles (10 cm³ and 65 cm³ mixing volumes), as well as a mechanical stirrer. 16,23,25,28,39 We also varied the input gallium quantity in the smaller mortar and pestle within the range used in our own and prior studies.^{17,27} We note that in most cases the details of the mixing process (e.g., input volume of LM, size of the mixing vessel, and mixing rate) are underreported, which can make replication of the material fabrication challenging. We decided to add SiO₂ particles because of several prior reports on their addition to LM,^{28,29} their common use to stabilize Pickering emulsions⁴³ and even aqueous foams,^{43–45} and their low-cost availability with near spherical shapes in several sizes spanning the \sim 0.8 to 10 μ m preferred range for stabilizing aluminum foams.⁴⁶ The exterior surfaces of the LM composites was relatively smooth without major features such as pores observed in "oxide-assisted" LM foams⁴² (see representative micrographs in Figure S4 of the Supporting Information), implying that current samples predominantly have closed-cell internal features. The cross-sectional electron micrograph in Figure 1a shows that mixing the filler particles in the liquid gallium results in the formation of many features with "moon-crater" appearance that corresponds to cross-sectioned near-spherical air bubbles with diameters ranging from \sim 5 µm to \sim 300 µm. We note that any internal features in

the LM containing air are "capsules" surrounded by the rapidly forming 1 to 3 nm thick oxide layer.

The entrapment of these microscopic air capsules within the metal reduces the density of the LM composite. The bar plot in **Figure 1b** shows that the model, shape, and size of the mortar and pestle (see images in **Figure 1d**) has a relatively minor influence on the density (variation below ~0.25 g cm⁻¹ or ~5% variation) of the LM-SiO₂ composites. However, when we prepared the material using a mechanical stirrer, the density was substantially lower than samples prepared by hand-mixing (decrease of ~0.5 g cm⁻¹ or ~10%). Furthermore, the cross-sectional electron micrograph in **Figure 1c** shows that the internal structure of the mechanically-mixed composite is considerably more disordered than that of the manually-mixed equivalent. Rather than primarily spherical capsules, the mechanically-mixed sample contains many irregularly-shaped voids and features with a "dark" appearance in the micrographs that indicates that they are elongated voids ("deep channels") from which the image-forming secondary electrons cannot escape.⁴⁷ To gain more insight into these observations, we systematically investigate manually-mixed (small mortar and pestle with 5 g Ga input) and mechanically-mixed composites with a varied volume fraction of SiO₂ particles with three different size distributions.

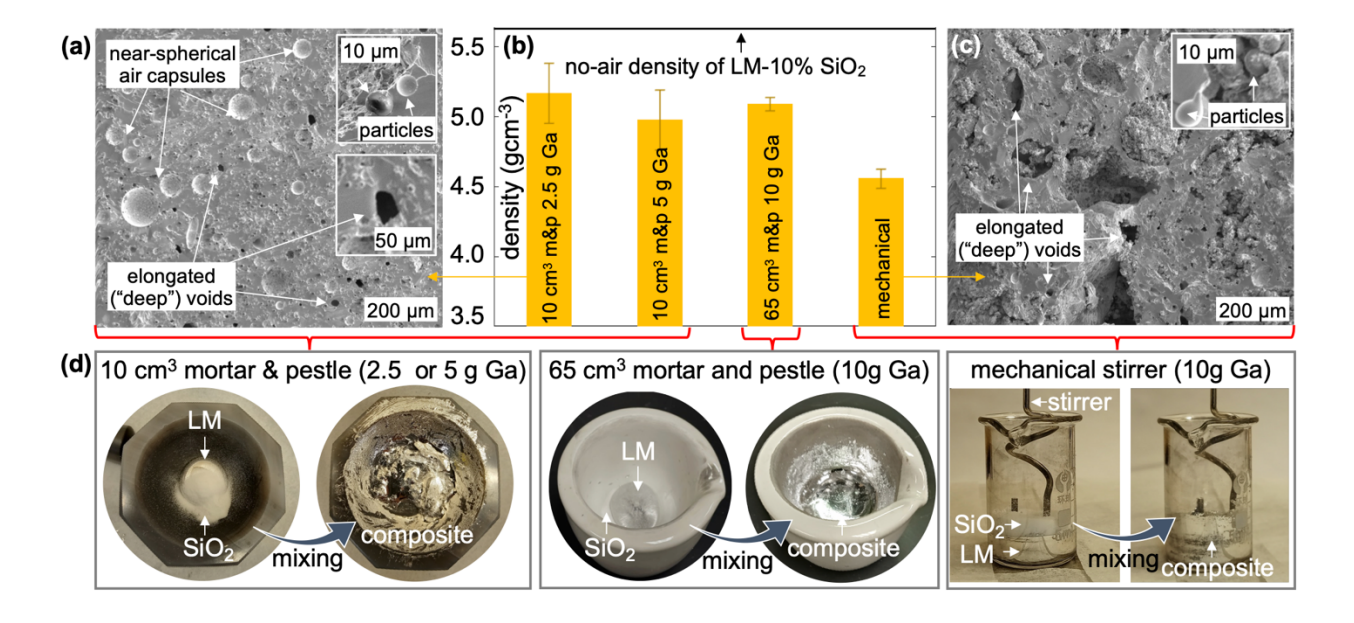


Figure 1. Impact of fabrication method on density and internal structure of LM mixed for 20 minutes with 10% volume fraction of 5 μm SiO₂ particles: (a) cross-sectional electron micrograph of manually-mixed liquid metal composite (small mortar and pestle ("m&p") with 5 g of gallium), (b) the density of the composites made using the indicated four approaches (referenced in (d)), (c) cross-sectional electron micrograph of mechanically-mixed liquid metal composite, and (d) images of the small mortar and pestle with 5 g of gallium (2.5 g was alternatively used for some experiments), the larger mortar and pestle with 10 g of gallium, and of mechanical stirrer with 10 g of gallium. Detailed description of each method is included in the Experimental Section.

2.2 Manually-mixed LM composites with SiO₂ particles

We used the small mortar and pestle to fabricate gallium composites containing 1%, 2.5%, 5%, 10%, and 20% volume fractions of the SiO_2 particles with average diameters of 0.8, 5, and 10 μ m (see micrographs and particle size distributions in the Supporting Information). The first noticeable observation we made during mixing was that smaller particles take much longer to integrate

entirely within the LM compared to larger particles. For example, the plot in **Figure 2a** shows that completely mixing in 20% volume fraction of the 0.8 µm SiO₂ particles took, on average, about 19 minutes. In contrast, the same concentration of the 10 µm particles took around 3.5 minutes to mix. Ren et al. ¹⁶ also observed that it is much more difficult to mix in smaller particles (100 nm vs. 70 µm iron) into LM as the mixture with the former becomes substantially more viscous and suggested that the increased surface area (for the same volume fraction) of the smaller particles could play a role in the process. These internalization times are impacted by the mortar and pestle characteristics, and to some extent, by sample-to-sample variation. For consistency, we subsequently compare the impact of particle size and volume fraction on the density of the samples mixed for 20 minutes. We note that the density of the samples is not impacted much by varying the mixing time between 10 and 30 minutes (see example results in Figure S3 of the Supporting Information).

The increase in the filler particle content decreases the composite density because SiO₂ is substantially lighter than gallium (~2.2 g cm⁻³ versus ~6 g cm⁻³). Furthermore, the plot in **Figure 2b** shows that the density of all the LM composites is lower than one calculated for any given volume fraction of the fillers with the assumption of no air entrapment ("no-air density"). Naturally, this observation demonstrates the internalization of microscale air capsules within the LM. As the volume fraction of the filler particles increases, so does the gap between the calculated "no-air" and measured densities. In other words, within the 1 to 20% volume fraction, the higher the filler particle concentration, the more air entrapment ("foaming") of the composite occurs (see Figure S2 in Supporting Information for estimated volume fraction of entrapped air).

Our results also demonstrate that mixing particles with lower diameters decreases the composite density, introducing more air capsules into the liquid. The density difference related to

the filler particle size can be substantial. For example, the densities of the composites with the 20% volume fraction of SiO₂ (all mixed for 20 minutes) with average diameters of 0.8, 5, and 10 μ m are 3.9, 4.2, and 4.5 g cm⁻¹, respectively. Thus, our density measurements demonstrate that air internalization into manually-mixed LM composites increases with increasing content and decreasing size of filler particles (*i.e.*, the lowest density occurs for the 20% volume fraction of 0.8 μ m SiO₂).

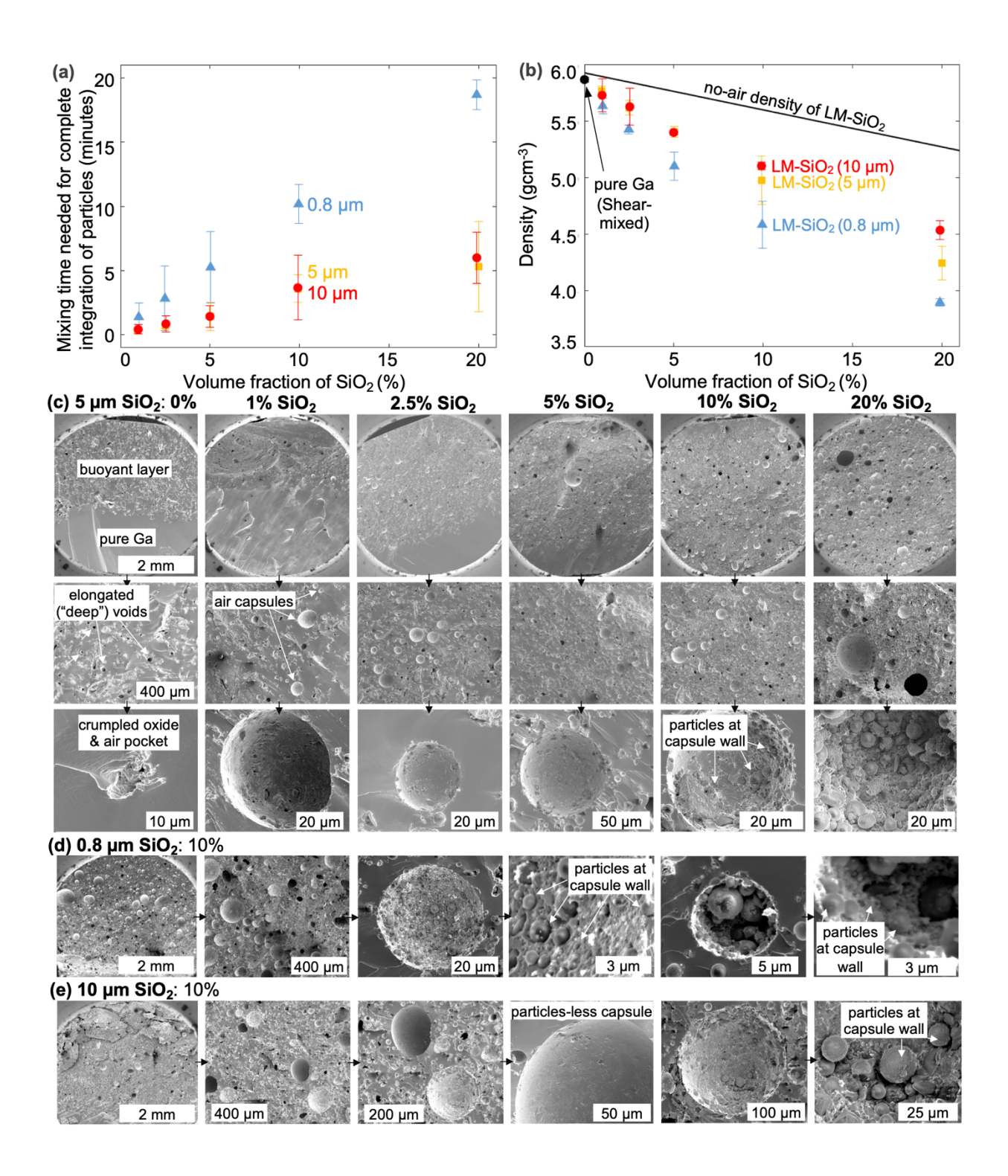


Figure 2. Manually-mixed LM-SiO₂ composites: (a) time required to entirely mix filler particles into the LM using the small mortar and pestle, (b) the density of the composites with varying

volume fraction and size of the fillers mixed for 20 minutes, and cross-sectional micrographs of the LM-SiO₂ composites with (c) 5 μm, (d) 0.8 μm, and (e) 10 μm average diameters.

The cross-sectional electron micrographs in Figure 2c-e visually corroborate the increase in microscale air capsule quantity with increasing SiO₂ particle volume content and decreasing average diameter. A foam of the capsules forms during manual mixing even without any SiO₂ particle addition (see "0%" volume fraction images) due to internalization of the oxide microflakes from the external interface between LM and air.³⁶ The oxide flakes are crumpled into threedimensional "particles" that, as indicated by the buoyancy of the particle layer (see Figure 2c "0%"), often entrap mostly irregularly shaped air pockets of various sizes (the buoyant layer also forms with addition of low volume fraction of particles, while at higher volume fractions the foam fills up the entire sample height). Within 20 minutes of mixing pure gallium, enough oxide flakes are incorporated to entrap larger, irregularly shaped, and elongated air capsules. In contrast, the addition of even only 1% volume fraction of the 5 µm SiO₂ particles leads to the formation of many near-spherical air capsules. The micrographs also show that increasing particle volume fraction and decreasing their average diameter increases the number of the near-spherical air capsules (thereby reducing density) and the accumulation of particles at the walls of the capsules. Next, we evaluate how these characteristics are altered by switching to the mechanical stirring of the composites.

2.3 Mechanically-mixed LM composites with SiO₂ particles

We used the mechanical stirrer to fabricate gallium composites containing the same volume fractions of the SiO₂ particles (1, 2.5, 5, 10, and 20%), but only those with an average diameter of 5 μm. The SiO₂ particles and gallium were pre-mixed in a mortar and pestle for 2 minutes to prevent aerosolizing, followed by mechanically stirring at 600 rpm for 20 minutes. Our attempts at mixing in the 0.8 μm particles with the LM using this approach did not yield a macroscopically homogenous composite. Furthermore, the 10 μm particles produce similar results to the 5 μm particles, so we focused on the detailed investigation of composites with the latter. Despite the difference in mixing rates (~120 rpm for manual and 600 rpm for mechanical stirring), the time to fully integrate the 5 μm particles into LM using mechanical mixing for the higher volume fractions was on the order of 5 to 7 minutes (*i.e.*, not shorter than manual mixing). Consequently, comparison by the total number of mixing rotations was not possible, and we selected to compare the impact of volume fraction on the density of the samples mixed for 20 minutes.

As in the case of the manually-mixed composites, the increase in the particle volume fraction decreased the composite density and did so far below the calculated "no-air" density (see **Figure 3a**). In addition, the density of the mechanically-mixed composites was 0.3 to 0.5 g cm⁻³ lower than those with equivalent input composition made manually. This systematic offset in the density correlates with the presence of elongated air capsules, an example of which is clearly shown in the cross-sectional micrograph in **Figure 3b**. In this example, the cross-sectioning occurred across the longer dimension of the void, highlighting its elongated nature. In most cases, these elongated features are cut along the smaller dimension, giving them the "deep void" dark appearance in the micrographs. Such features likely form when surface waves on the external air-liquid interface crest and internalizing air bubbles are "stretched" by rapidly moving liquid. Similarly, internalized

larger spherical air capsules might be deformed by liquid shear forces caused by rapid stirring. Many such features form with crumpled oxide flakes during mechanical stirring for 20 minutes without any particle addition (see "0%" images in **Figure 3c**). Continuing the fast stirring of the pure gallium for even another 100 minutes will lead to the internalization of more oxide and air but will decrease the density from 5.6 g cm⁻³ (after 20 minutes of stirring) to 4.8 g cm⁻³. Impressively, the addition of 20% volume fraction of the 5 μm SiO₂ particles enhances foaming so that in just 20 minutes of mixing the density decreases to 4.2 g cm⁻³ (manual mixing) and 3.7 g cm⁻³ (mechanical mixing). In both cases, cross-sectional micrographs reveal that the particles accumulate on the walls of the capsules. In the case of the mechanically-mixed composites, the particles also appear to aggregate into large, oxide-bridged clusters within the voids (see, for example, the close-up image for "10% SiO₂" in **Figure 3c** or **Figure 3b**). Next, we discuss potential microscopic mechanisms underlying these trends.

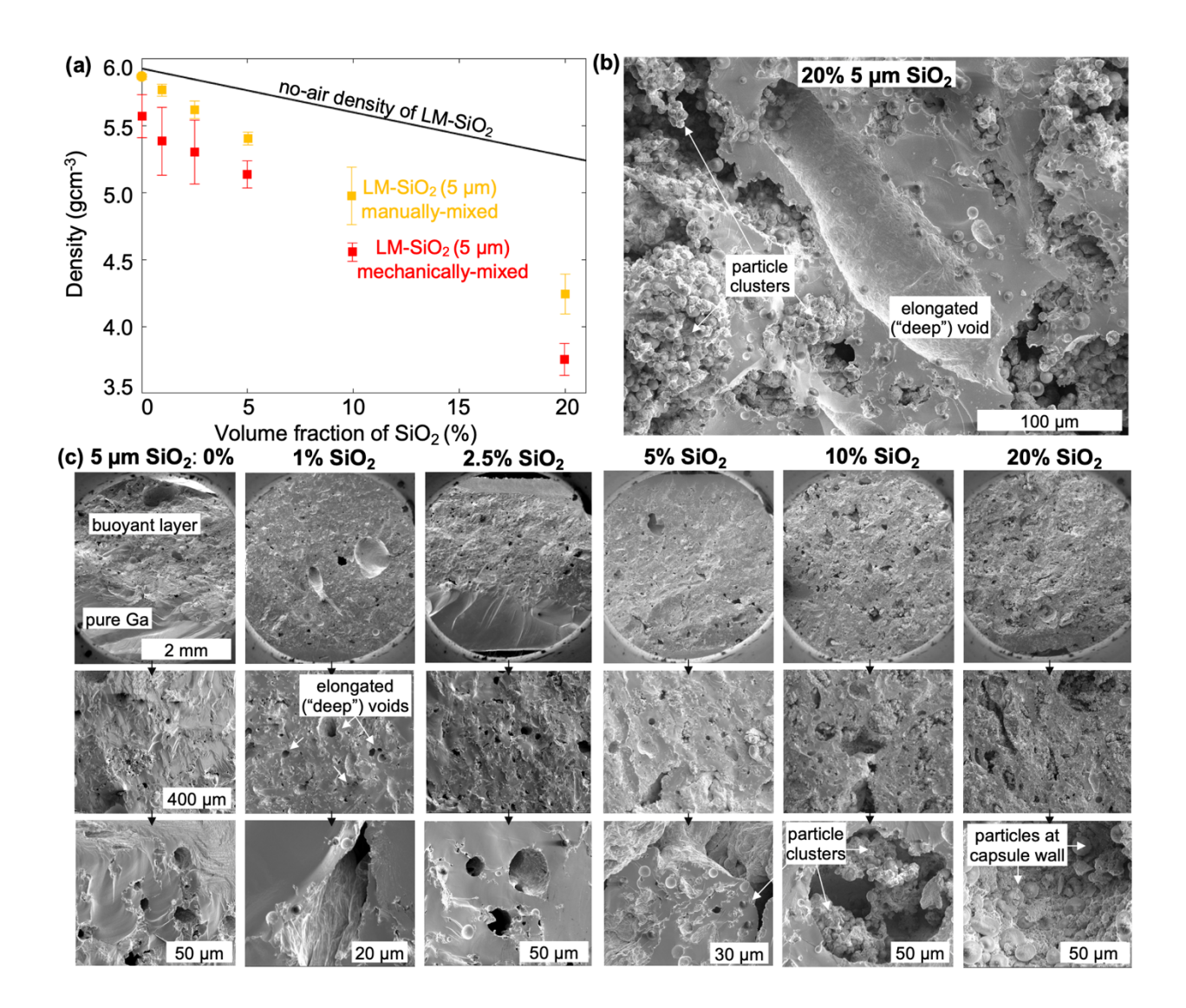


Figure 3. Mechanically-mixed LM-SiO₂ composites: **(a)** the density of the composites with varying volume fractions of the 5 μm SiO₂ particles, and cross-sectional micrographs of the LM-SiO₂ composites with **(b)** 20% volume fraction and **(c)** with varying volume fractions of the particles. The large micrograph in (b) reveals the cross-section of an elongated ("deep") void along the void's longer dimension.

2.4 Discussion of possible microscale mechanisms contributing to particle-driven LM foaming enhancement

Besides stabilizing liquid metal foams, ^{36,46,48} solid particles can cause foaming in rivers, distillation towers, oil-well drilling, pulping, and even radioactive waste. ^{49,50} However, as opposed to aqueous foams, ^{50–54} there is still debate in the literature on how particles help to stabilize highmelting point metal foams. ⁴⁶ The process is likely to be further complicated in the case of gallium-based LMs by the rapidly forming oxide. There are two commonly used explanations for particles promoting foam stability. First is the creation of a barrier against coalescence by particles accumulated on the internal liquid-gas interfaces, which in case of LMs provide additional mechanical strength over capsule walls consisting only of the thin oxide (see **Figure 4a** and **b**). Second is the forced bubble separation and retardation of liquid drainage by particle networks between the bubbles (see **Figure 4c**). ^{46,49,50} Next, we discuss these two processes in the context of our experimental observations.

If particles are only partially wetted by a liquid, it is thermodynamically favorable for them to accumulate on air-liquid interfaces.⁴³ To form a barrier against bubble coalescence in aqueous foams, particles must have a specific range of wetting properties that allows them to be placed at the internal gas-liquid interfaces.^{49,50} These wetting property arguments, however, are not readily translated from aqueous liquids to gallium-based liquid metals due to the solid layer of gallium oxide that forms on the LM. In particular, aqueous foams are optimally stabilized by mildly hydrophilic particles (contact angles of ~70-86°)⁵⁰ and are destabilized (collapsed) by hydrophobic particles (contact angles greater than 90°).⁴⁹ In contrast, bare gallium-based liquid metals do not easily wet most materials (*i.e.*, oxide-free LM has contact angles greater than 120° for materials ranging from glass to Teflon),⁵⁵⁻⁵⁷ although the oxide can adhere to nearly any flat surface.⁵⁸ Our

observation of SiO₂ particles enhanced LM foaming can be reconciled with these high contact angles by pointing out the alternative LM "wetting" and encapsulation mechanism. Specifically, nearly any particles can be "wetted" (*i.e.*, partially or fully encapsuled) by the liquid metal during mixing through the adherence of multiple patches of LM oxide on their surface. As illustrated in **Figure 4d**, the oxide-patches locally make the area more easily wettable by the LM.¹¹ This mechanism can explain the variety of encapsulation degrees of the SiO₂ particles located at the interface between the LM and the air capsules in micrographs in **Figure 4d**. We note that the oxide also forms at the internal air-liquid metal interfaces and can alone stabilize the capsules of a variety of sizes as evidenced by the occasional mostly "particle-less capsules" shown in micrographs in **Figure 4a** and **Figure 2e**. The oxide can be easily identified by its surface that contains nanoscale and microscale wrinkles^{7,59}. However, the self-passivating oxide film is only \approx 3 nm thick, so can readily be ruptured by, for example, shearing forces during mixing. Thus, the particles should promote LM foam stability by enhancing the strength of the capsule walls that consist mostly of the relatively weak oxide film.

Prior literature suggests that foaming occurs preferentially for a specific window of added particle sizes for both the high-melting-point metal foams (sub-micrometer to tens of micrometers)^{46,60–62} and aqueous foams (tens of nanometers to micrometers).⁵⁰ The preferred particle volume fraction is ~1 to 20%, above which the mixture becomes too viscous to process.⁴⁶ Similarly, particles with size below ~0.8 μm are noted as too difficult (*i.e.*, making the solution too viscous) to mix into high-melting-point liquid metals.⁴⁶ For gallium-based liquid metals, oxide-patches might not readily adhere on the high curvature nanoparticles, making them challenging to internalize. For example, prior studies show that gallium-based liquid metals (with the native oxide) do not stick to surfaces sparsely coated with silica nanoparticles.⁵⁸ For the particle sizes that

do mix in, our results indicate that the smallest particles promote the highest foaming degree of the LM. As evident from the cross-sectional micrographs in **Figures 2**, the 0.8 µm particles form more complete films on the capsule walls, thus making a stiffer wall that provides a better barrier to deformation or coalescence than one with isolated larger particles. We also highlight that the capsules in our LM foams have diameters mostly below 100 µm, which is a similar size to bubbles in particle-stabilized aqueous foams. ^{43–45,63} This capsule size range makes the formation of barriers consisting of smaller particles easier. The reduced chance of capsule coalescences associated with the 0.8 µm stiffened walls likely decreases the probability of formation of large air voids that can easily separate from the LM sample. Thus, while the amount of air forced to mix with the LM is likely similar for a given mixing approach, the smaller particles are more effective at stabilizing and retaining the gas within the liquid. Besides providing a better barrier to coalescence during direct capsule-capsule contact than the oxide alone, the particles within the liquid can also prevent the capsules from coming in contact.

In the LM foams, particles in-between capsules can form networks with crumbled oxide flakes that help stabilize the foam in three ways. First, such particle-oxide flake chains (highlighted in **Figure 4c)** can push against capsules and prevent them from coming into direct contact. Second, such networks can also slow drainage of the LM from in-between the capsules. Third, we speculate that such networks of particles, along with the capsules, accumulate in the buoyant layer near the top surface of the LM foam. We hypothesize that this layer in turn provides additional foam stability by preventing the buoyancy-driven escape of newly trapped air bubbles.

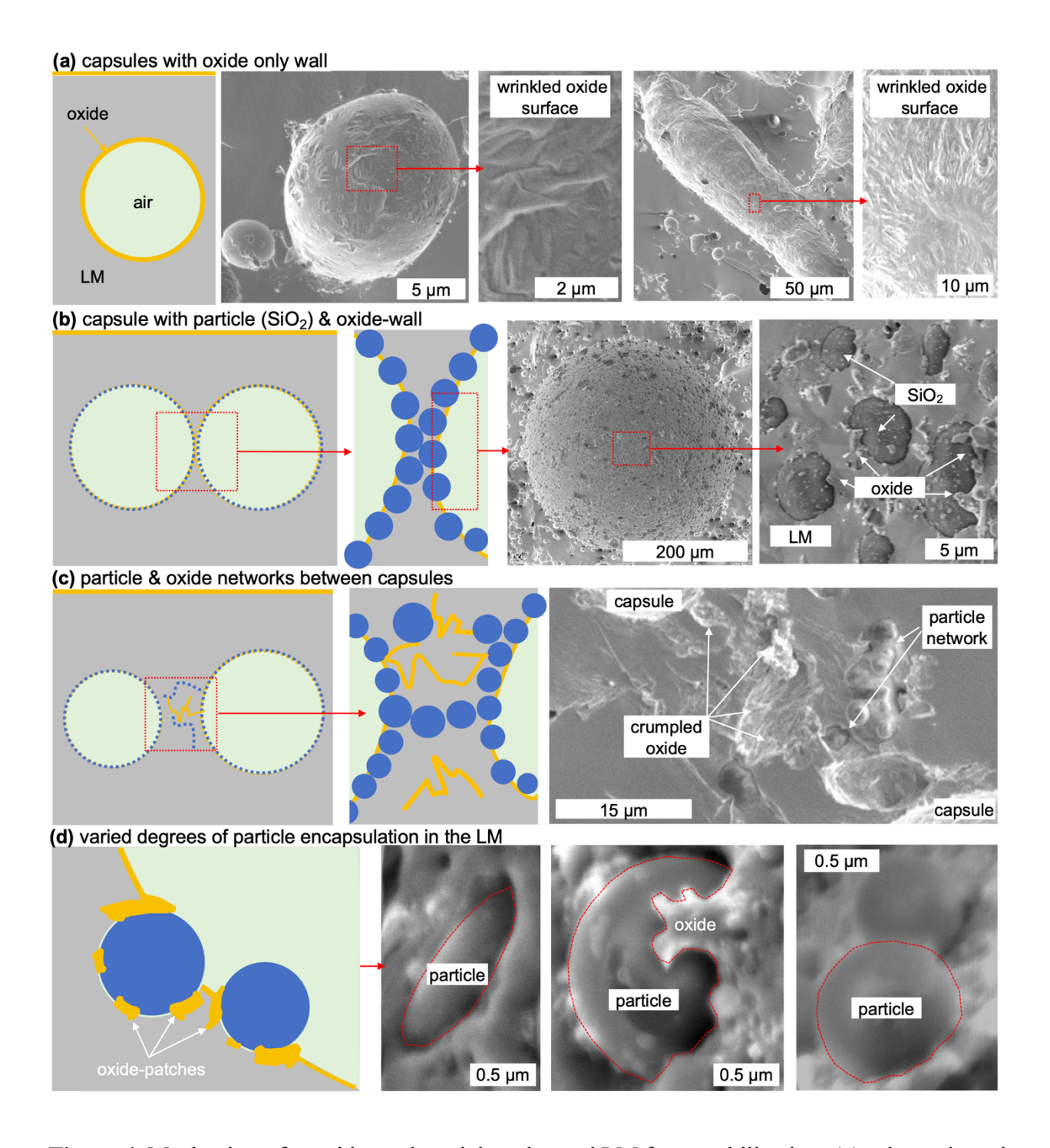


Figure 4. Mechanisms for oxide- and particle-enhanced LM foam stabilization: (a) schematic and micrograph of a capsules with variety of sizes and with a wall consisting mostly of gallium oxide, (b) schematic and micrographs of a capsule with a wall consisting of oxide and particles, which forms a barrier to direct capsule contact and coalescence, (c) schematic and micrograph of particle

and oxide networks in-between capsules that can prevent them from coming into contact, and (d) schematic and micrographs of oxide-patched mediated "wetting" and encapsulation of particles by the LM which leads to a variety of encapsulation states illustrated in the micrographs.

2.5 Thermal conductivity of the multiphase LM composites

The plot in Figure 5a shows the effective thermal conductivity (that includes the thermal contact resistances to the samples) of the multiphase LM composites with varied particles size and volume fraction made either through manual or mechanical mixing. Since the particles are thermally insulating (~1 W m⁻¹ K⁻¹) and their addition is associated with increased air entrapment, the thermal conductivity decreases with increasing particle volume fraction. As the composite density, the thermal conductivity is also lower for composites containing the smaller particles and those made through mechanical stirring. In fact, the plot in Figure 5b shows that the thermal conductivity decreases linearly with decreasing density of the composites. In other words, the higher is the air content of the composites, the lower is their thermal conductivity and density. A very similar trend between density and thermal conductivity is also displayed by the "oxide-only" LM foams we originally fabricated through stirring pure LM at 600 rpm in air for 120 minutes.³⁶ However, the extended period (20 vs. 120 minutes) of rapid mixing creates a substantial content of the crumpled oxide flakes, which leads to ~2 to 5 W m⁻¹ K⁻¹ lower thermal conductivity as compared to the LM-SiO₂ composites with matching density. We also highlight that the thermal conductivity and density of the "oxide-only" LM foams saturates with mixing time at ~18 W m⁻¹ K⁻¹ and 4.8 g cm⁻³. In contrast, the properties of the LM-SiO₂ composites can be further tuned and provide some improvement over the "oxide-only" foams. For example, the LM composites with 20% of 5 µm SiO₂ particles has same thermal conductivity as the "saturated" oxide-only foams

(*i.e.* 18 W m⁻¹ K⁻¹) but substantially lower density of 4.2 g cm⁻³. In other words, in a microelectronics package, using the particle-enabled composite would provide same thermal performance while making the package lighter. We also note that if higher thermal conductivities are desired, the SiO₂ should be replaced with more thermally conductive particles such as tungsten or silicon carbide.^{11,27}

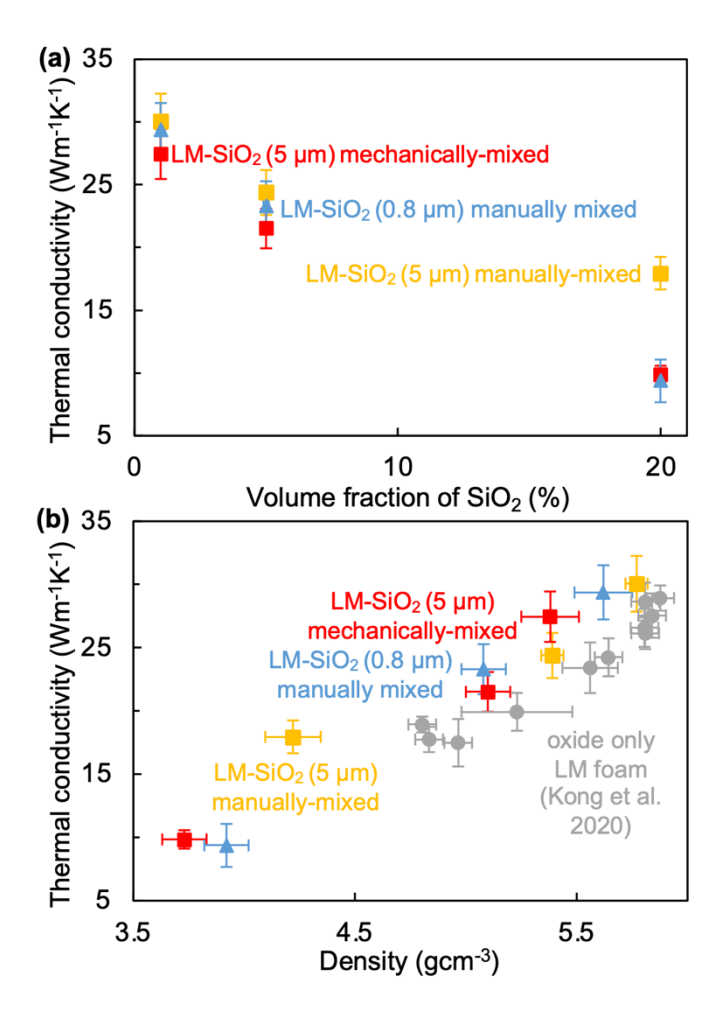


Figure 5. The effective thermal conductivity of the multiphase LM composites plotted against (a) volume fraction of SiO2 particles and (b) their density; the latter includes data on "oxide-only" LM foams fabricated through stirring LM in air at 600 rpm for 120 minutes made by Kong et al.³⁶ (no particles).

3. Conclusions

We studied the basics of the fabrication of multiphase LM composite with solid and fluid fillers. Our experiments demonstrated that the blending of particles results in the unintentional incorporation of air bubbles into the composite and that the quantity of the entrapped air depends on the mixing method (up to 30% volume fraction, see Supporting Information). In particular, manually mixing the LM with particles in a mortar and pestle incorporates a smaller air volume than mechanical stirring. Manual mixing also yields many more near-spherical air capsules than mechanical-mixing, which creates numerous elongated voids. We also demonstrated that decreasing the particle size and increasing their volume fraction decreases the composite density and thermal conductivity (i.e., increases air entrapment). Electron micrographs indicate that the smaller SiO₂ particles (0.8 μm) can assemble more complete barriers than larger ones (5 μm and 10 μm) on the microscopic air capsules (diameters mostly below 100 μm). Such particle-enhancedcapsule walls likely provide a stiffer and better barrier than oxide-only walls against direct bubble coalescence through which foams can collapse, thus leading to lower density composites. The particles, along with crumpled oxide flakes, within the liquid metal also likely help to separate air capsules, preventing their direct contact.

Our results can be employed to guide adjustment of the composition and fabrication method of LM composite to promote the formation of more paste-like or foam-like materials. To make pastes with minimized air content that, for example, have enhanced thermal (as showed in our experiments) or electrical conductivity, larger conductive particles should be mixed into the LM manually. In contrast, the LM should be mixed with smaller particles to make foams with maximized air content. The mixing method can be used to adjust the internal structure of the foam

with manual mixing yielding more near-spherical capsules and mechanical mixing more elongated features. Adding particles creates foams faster (20 minutes vs. 120 minutes) and makes substantially lighter foams (e.g., 3.7 g cm⁻³ vs. 4.8 g cm⁻³) than previously employed stirring pure LM in air. Looking outward, we anticipate that studies on non-spherical particles and/or particles with surface texture could provide additional insights on the creation of paste-like versus foamlike LM composites.

4. Experimental Section

We fabricated the various liquid metal composites by melting the solid gallium (99.99% from Rotometals) on a hot plate set to 60°C (which results in a LM temperature of ~50 to 55°C) and mixing with SiO₂ (US Research Nanomaterials, Inc). The SiO₂ particles were mostly spherical with average diameters of 0.8 µm, 5 µm, and 10 µm (see particle size distributions in the Supporting Information) and are utilized as received from the manufacturer. We note that the surface functionalization of the particles does not have major impact on the LM wetting and mixing in process, 7,11 which occurs through the previously described oxide patch adhesion and wetting mechanism.¹¹ We fabricated samples containing 1%, 2.5%, 5%, 10%, 20% volume fraction of filler particles in gallium. We mixed the filler particles with LM in four ways, including 10 cm³ ("small") mortar and pestle (VWR Mortars and Pestle, mortar Top O.D. x I.D.: 51x38 mm and height 29 mm, pestle O.D. 13.5 mm, material: agate; VWR catalog number 89037-484) with either 2.5 or 5 g of gallium, 65 cm³ ("larger") porcelain mortar and pestle (Coorstek Mortar, mortar: O.D. x I.D.: 80 x 53 mm, pestle O.D. 38 mm, Mfr. No. 60313, Coorstek Pestle, 130 mm, Mfr. No. 60314) with 10 g of gallium, and a mechanical stirrer (removed from Orment Led Lighting Epoxy Resin Electric Mixer made of stainless steel) rotating at 600 rpm with 10 g of gallium in a 5 mL

borosilicate glass beaker (Lipovolt Chemistry Laboratory Borosilicate Beaker). The filler particles were weighed, added into the mortar, and mixed manually at approximately 120 rpm. To prevent loss of particles by aerosolization and potential associated inhalation hazard, we manually premixed the particles into the LM for 2 minutes before rapid mechanical stirring at 600 rpm. We prepared three individual samples (each made by a different team member) for each composition and mixing procedure and report the results with a ~80% confidence interval specified by the t-distribution (2 standard deviations for a set of 3 samples).

We measured the density of the multiphase LM composites using the Archimedes principle. The LM samples were solidified and weighed in air followed by weighing while suspended in water (using a 40 mL beaker of deionized water). All electron micrographs were collected using FEI Nova 200 FIB-SEM with a 5 kV accelerating voltage and 0.4 nA current after the manual cutting of frozen samples using a razor blade. Based on the smooth appearance of the local cross-sectional area, we infer that the razor blade melts the top ~0.1 mm region at the line of contact, but does not impact the cross section below. Upon impact of a rapid force onto the razor blade top, most samples fracture along the razor blade. We measured the effective thermal conductivity of the about 2.8 mm thick samples using stepped bar apparatus based on ASTM D5470 standard. Ale the devices and measurement protocols are described in depth in our prior work. Section we note that when unperturbed the samples do not undergo spontaneous geometrical change over time so can be stored for extended periods of time.

ASSOCIATED CONTENT

Supporting Information The Supporting Information is available free of charge on the ACS

Publications website. The particle size distributions, calculated entrapped air volume fractions in

the composites, data on the effect of mixing time on entrapped air volume fraction, and additional

electron micrographs are available.

AUTHOR INFORMATION

Corresponding Author

*email: konradr@asu.edu and rywang@asu.edu

Author Contributions

The manuscript was written through contributions of all authors. All authors have given approval

to the final version of the manuscript.

Funding Sources

This research was funded by National Science Foundation Division of Civil, Mechanical and

Manufacturing Innovation grant 2032415. NUHS was supported by the Fulbright-HEC

Scholarship program.

ACKNOWLEDGMENT

22

The authors gratefully acknowledge the use of the microscopy equipment within the LeRoy Eyring Center for Solid State Science at Arizona State University.

REFERENCES

- (1) Daeneke, T.; Khoshmanesh, K.; Mahmood, N.; de Castro, I. A.; Esrafilzadeh, D.; Barrow, S. J.; Dickey, M. D.; Kalantar-Zadeh, K. Liquid Metals: Fundamentals and Applications in Chemistry. *Chem Soc Rev* **2018**, *47* (11), 4073–4111.
- (2) Chen, S.; Wang, H.-Z.; Zhao, R.-Q.; Rao, W.; Liu, J. Liquid Metal Composites. *Matter* **2020**, *2* (6), 1446–1480.
- (3) Malakooti, M. H.; Bockstaller, M. R.; Matyjaszewski, K.; Majidi, C. Liquid Metal Nanocomposites. *Nanoscale Adv* **2020**, *2* (7), 2668–2677.
- (4) Chen, S.; Deng, Z.; Liu, J. High Performance Liquid Metal Thermal Interface Materials. *Nanotechnology* **2020**, *32*, 092001. https://doi.org/10.1088/1361-6528/abcbc2.
- (5) Lu, Y.; Hu, Q.; Lin, Y.; Pacardo, D. B.; Wang, C.; Sun, W.; Ligler, F. S.; Dickey, M. D.; Gu, Z. Transformable Liquid-Metal Nanomedicine. *Nat Commun* **2015**, *6* (10066), 1–10.
- (6) Handschuh-Wang, S.; Stadler, F. J.; Zhou, X. Critical Review on the Physical Properties of Gallium-Based Liquid Metals and Selected Pathways for Their Alteration. *The Journal of Physical Chemistry C* **2021**, *125* (37), 20113–20142.
- (7) Doudrick, K.; Liu, S.; Mutunga, E. M. E. M.; Klein, K. L. K. L.; Damle, V.; Varanasi, K. K. K.; Rykaczewski, K. Different Shades of Oxide: From Nanoscale Wetting Mechanisms to Contact Printing of Gallium-Based Liquid Metals. *Langmuir* **2014**, *30* (23), 6867–6877. https://doi.org/10.1021/la5012023.
- (8) Dickey, M. D. Emerging Applications of Liquid Metals Featuring Surface Oxides. *ACS Appl Mater Interfaces* **2014**, *6* (21), 18369–18379. https://doi.org/10.1021/am5043017.
- (9) Neumann, T. v; Dickey, M. D. Liquid Metal Direct Write and 3D Printing: A Review. *Adv Mater Technol* **2020**, 2000070.
- (10) Larsen, R. J.; Dickey, M. D.; Whitesides, G. M.; Weitz, D. A. Viscoelastic Properties of Oxide-Coated Liquid Metals. *J Rheol (N Y N Y)* **2009**, *53* (6), 1305–1326.
- (11) Kong, W.; Wang, Z.; Wang, M.; Manning, K. C.; Uppal, A.; Green, M. D.; Wang, R. Y.; Rykaczewski, K. Oxide-Mediated Formation of Chemically Stable Tungsten–Liquid Metal Mixtures for Enhanced

- Thermal Interfaces. *Advanced Materials* **2019**, *31* (44). https://doi.org/10.1002/adma.201904309.
- (12) Li, G.; Ji, Y.; Wu, M.; Ma, H. Highly Conductive Thermal Paste of Liquid Matal Alloy Dispersed with Copper Particles. In *Proceedings of the ASME 2016 heat transfer summer conference*; Wahington DC, 2016.
- (13) Tang, J.; Zhao, X.; Li, J.; Guo, R.; Zhou, Y.; Liu, J. Gallium-Based Liquid Metal Amalgams: Transitional-State Metallic Mixtures (TransM2ixes) with Enhanced and Tunable Electrical, Thermal, and Mechanical Properties. *ACS Appl Mater Interfaces* **2017**, *9* (41), 35977–35987. https://doi.org/10.1021/acsami.7b10256.
- (14) Tutika, R.; Zhou, S. H.; Napolitano, R. E.; Bartlett, M. D. Mechanical and Functional Tradeoffs in Multiphase Liquid Metal, Solid Particle Soft Composites. Adv Funct Mater 2018, 28 (45), 1804336. https://doi.org/10.1002/adfm.201804336.
- (15) Ralphs, M. I. M. I.; Kemme, N.; Vartak, P. B. P. B.; Joseph, E.; Tipnis, S.; Turnage, S.; Solanki, K. N.; Wang, R. Y. R. Y.; Rykaczewski, K. In Situ Alloying of Thermally Conductive Polymer Composites by Combining Liquid and Solid Metal Microadditives. *ACS Appl Mater Interfaces* **2018**, *10* (2), 2083–2092. https://doi.org/10.1021/acsami.7b15814.
- (16) Ren, L.; Sun, S.; Casillas-Garcia, G.; Nancarrow, M.; Peleckis, G.; Turdy, M.; Du, K.; Xu, X.; Li, W.; Jiang, L.; Dou, S. X.; Du, Y. A Liquid-Metal-Based Magnetoactive Slurry for Stimuli-Responsive Mechanically Adaptive Electrodes. *Advanced Materials* **2018**, *30* (35), 1802595. https://doi.org/10.1002/adma.201802595.
- (17) Carle, F.; Bai, K.; Casara, J.; Vanderlick, K.; Brown, E. Development of Magnetic Liquid Metal Suspensions for Magnetohydrodynamics. *Phys Rev Fluids* **2017**, *2* (1), 13301.
- (18) Guo, R.; Wang, X.; Chang, H.; Yu, W.; Liang, S.; Rao, W.; Liu, J. Ni-Galn Amalgams Enabled Rapid and Customizable Fabrication of Wearable and Wireless Healthcare Electronics. *Adv Eng Mater* **2018**, *20* (10), 1800054.
- (19) Ralphs, M.; Kong, W.; Wang, R. Y.; Rykaczewski, K. Thermal Conductivity Enhancement of Soft Polymer Composites through Magnetically Induced Percolation and Particle—Particle Contact Engineering. *Adv Mater Interfaces* **2019**, *6* (6), 1801857. https://doi.org/10.1002/admi.201801857.
- (20) Daalkhaijav, U.; Yirmibesoglu, O. D.; Walker, S.; Mengüç, Y. Rheological Modification of Liquid Metal for Additive Manufacturing of Stretchable Electronics. *Adv Mater Technol* **2018**, *3* (4), 1700351. https://doi.org/10.1002/admt.201700351.
- (21) Tang, J.; Zhao, X.; Li, J.; Zhou, Y.; Liu, J. Liquid Metal Phagocytosis: Intermetallic Wetting Induced Particle Internalization. *Advanced Science* **2017**, *4* (5), 1700024. https://doi.org/10.1002/advs.201700024.
- (22) Wang, X.; Guo, R.; Yuan, B.; Yao, Y.; Wang, F.; Liu, J. Ni-Doped Liquid Metal Printed Highly Stretchable and Conformable Strain Sensor for Multifunctional Human-Motion Monitoring. In

- 2018 40th Annual International Conference of the IEEE Engineering in Medicine and Biology Society (EMBC); IEEE, 2018; pp 3276–3279.
- (23) Lin, Z.; Liu, H.; Li, Q.; Liu, H.; Chu, S.; Yang, Y.; Chu, G. High Thermal Conductivity Liquid Metal Pad for Heat Dissipation in Electronic Devices. *Appl Phys A Mater Sci Process* **2018**, *124* (5), 368. https://doi.org/10.1007/s00339-018-1778-z.
- (24) Tavakoli, M.; Malakooti, M. H.; Paisana, H.; Ohm, Y.; Green Marques, D.; Alhais Lopes, P.; Piedade, A. P.; de Almeida, A. T.; Majidi, C. EGaln-Assisted Room-Temperature Sintering of Silver Nanoparticles for Stretchable, Inkjet-Printed, Thin-Film Electronics. *Advanced Materials* **2018**, *30* (29), 1801852. https://doi.org/10.1002/adma.201801852.
- (25) Wang, X.; Yao, W.; Guo, R.; Yang, X.; Tang, J.; Zhang, J.; Gao, W.; Timchenko, V.; Liu, J. Soft and Moldable Mg-Doped Liquid Metal for Conformable Skin Tumor Photothermal Therapy. *Adv Healthc Mater* **2018**, *7* (14), 1800318. https://doi.org/10.1002/adhm.201800318.
- (26) A. de Castro, I.; Chrimes, A. F.; Zavabeti, A.; Berean, K. J.; Carey, B. J.; Zhuang, J.; Du, Y.; Dou, S. X.; Suzuki, K.; Shanks, R. A. A Gallium-Based Magnetocaloric Liquid Metal Ferrofluid. *Nano Lett* **2017**, *17* (12), 7831–7838.
- (27) Kong, W.; Wang, Z.; Casey, N.; Korah, M. M.; Uppal, A.; Green, M. D.; Rykaczewski, K.; Wang, R. Y. High Thermal Conductivity in Multiphase Liquid Metal and Silicon Carbide Soft Composites. *Adv Mater Interfaces* **2021**, 2100069.
- (28) Chang, H.; Zhang, P.; Guo, R.; Cui, Y.; Hou, Y.; Sun, Z.; Rao, W. Recoverable Liquid Metal Paste with Reversible Rheological Characteristic for Electronics Printing. *ACS Appl Mater Interfaces* **2020**, *12* (12), 14125–14135.
- (29) Yuan, B.; Zhao, C.; Sun, X.; Liu, J. Lightweight Liquid Metal Entity. *Adv Funct Mater* **2020**, 1910709.
- (30) Li, F.; Kuang, S.; Li, X.; Shu, J.; Li, W.; Tang, S.; Zhang, S. Magnetically-and Electrically-Controllable Functional Liquid Metal Droplets. *Adv Mater Technol* **2019**, *4* (3), 1800694.
- (31) Wei, S.; Yu, Z.; Zhou, L.; Guo, J. Investigation on Enhancing the Thermal Conductance of Gallium-Based Thermal Interface Materials Using Chromium-Coated Diamond Particles. *Journal of Materials Science: Materials in Electronics* **2019**, *30* (7), 7194–7202. https://doi.org/10.1007/s10854-019-01038-0.
- (32) Sargolzaeiaval, Y.; Ramesh, V. P.; Neumann, T. V.; Miles, R.; Dickey, M. D.; Öztürk, M. C. High Thermal Conductivity Silicone Elastomer Doped with Graphene Nanoplatelets and Eutectic Galn Liquid Metal Alloy. *ECS Journal of Solid State Science and Technology* **2019**, *8* (6), P357–P362. https://doi.org/10.1149/2.0271906jss.
- (33) Ma, K. Q.; Liu, J. Nano Liquid-Metal Fluid as Ultimate Coolant. *Physics Letters, Section A* **2007**, *361* (3), 252–256. https://doi.org/10.1016/j.physleta.2006.09.041.
- (34) Zhao, L.; Chu, S.; Chen, X.; Chu, G. Efficient Heat Conducting Liquid Metal/CNT Pads with Thermal Interface Materials. *Bulletin of Materials Science* **2019**, *42* (4), 192. https://doi.org/10.1007/s12034-019-1872-7.

- (35) Wang, X.; Fan, L.; Zhang, J.; Sun, X.; Chang, H.; Yuan, B.; Guo, R.; Duan, M.; Liu, J. Printed Conformable Liquid Metal E-Skin-Enabled Spatiotemporally Controlled Bioelectromagnetics for Wireless Multisite Tumor Therapy. *Adv Funct Mater* **2019**, 1907063.
- (36) Kong, W.; Shah, N. U. H.; Neumann, T. V; Vong, M. H.; Kotagama, P.; Dickey, M. D.; Wang, R. Y.; Rykaczewski, K. Oxide-Mediated Mechanisms of Gallium Foam Generation and Stabilization during Shear Mixing in Air. *Soft Matter* **2020**, *16*, 5801–5805.
- (37) Zhang, M.; Liu, L.; Zhang, C.; Chang, H.; Zhang, P.; Rao, W. Self-Foaming as a Universal Route for Fabricating Liquid Metal Foams and Hollow Particles. *Adv Mater Interfaces* **2021**, 2100432.
- (38) Gao, J.; Ye, J.; Chen, S.; Gong, J.; Wang, Q.; Liu, J. Liquid Metal Foaming via Decomposition Agents. *ACS Appl Mater Interfaces* **2021**, *13* (14), 17093–17103.
- (39) Wang, H.; Yuan, B.; Liang, S.; Guo, R.; Rao, W.; Wang, X.; Chang, H.; Ding, Y.; Liu, J.; Wang, L. Plus-M: A Porous Liquid-Metal Enabled Ubiquitous Soft Material. *Mater Horiz* **2018**, *5* (2), 222–229.
- (40) Xu, Y.; Lin, Z.; Rajavel, K.; Zhao, T.; Zhu, P.; Hu, Y.; Sun, R.; Wong, C.-P. Tailorable, Lightweight and Superelastic Liquid Metal Monoliths for Multifunctional Electromagnetic Interference Shielding. *Nanomicro Lett* **2022**, *14* (1), 1–15.
- (41) Shah, N. U. H.; Kong, W.; Casey, N.; Kanetkar, S.; Wang, R. Y.-S.; Rykaczewski, K. Gallium Oxide-Stabilized Oil in Liquid Metal Emulsions. *Soft Matter* 2021, 17, 8269–8275. https://doi.org/10.1039/D1SM00982F.
- (42) Shah, N. U. H.; Kanetkar, S.; Uppal, A.; Dickey, M. D.; Wang, R. Y.; Rykaczewski, K. Mechanism of Oil-in-Liquid Metal Emulsion Formation. *Langmuir* **2022**, *38* (43), 13279–13287. https://doi.org/10.1021/acs.langmuir.2c02428.
- (43) Binks, B. P.; Horozov, T. S. Aqueous Foams Stabilized Solely by Silica Nanoparticles. *Angewandte Chemie International Edition* **2005**, *44* (24), 3722–3725.
- (44) Gonzenbach, U. T.; Studart, A. R.; Tervoort, E.; Gauckler, L. J. Stabilization of Foams with Inorganic Colloidal Particles. *Langmuir* **2006**, *22* (26), 10983–10988.
- (45) Gonzenbach, U. T.; Studart, A. R.; Tervoort, E.; Gauckler, L. J. Ultrastable Particle-stabilized Foams. *Angewandte Chemie International Edition* **2006**, *45* (21), 3526–3530.
- (46) Banhart, J. Metal Foams: Production and Stability. Adv Eng Mater 2006, 8 (9), 781–794.
- (47) Goldstein, J. I.; Newbury, D. E.; Michael, J. R.; Ritchie, N. W. M.; Scott, J. H. J.; Joy, D. C. *Scanning Electron Microscopy and X-Ray Microanalysis*; Springer, 2017.
- (48) Banhart, J. Manufacturing Routes for Metallic Foams. Jom 2000, 52 (12), 22–27.
- (49) Hunter, T. N.; Pugh, R. J.; Franks, G. v; Jameson, G. J. The Role of Particles in Stabilising Foams and Emulsions. *Adv Colloid Interface Sci* **2008**, *137* (2), 57–81.
- (50) Horozov, T. S. Foams and Foam Films Stabilised by Solid Particles. *Curr Opin Colloid Interface Sci* **2008**, *13* (3), 134–140.

- (51) Prud'homme, R. Foams: Theory: Measurements: Applications; Routledge, 2017.
- (52) Shirtcliffe, N. J.; McHale, G.; Newton, M. I.; Perry, C. C. Intrinsically Superhydrophobic Organosilica Sol– Gel Foams. *Langmuir* **2003**, *19* (14), 5626–5631.
- (53) Binks, B. P. Particles as Surfactants—Similarities and Differences. *Curr Opin Colloid Interface Sci* **2002**, *7* (1–2), 21–41.
- (54) Murray, B. S.; Ettelaie, R. Foam Stability: Proteins and Nanoparticles. *Curr Opin Colloid Interface Sci* **2004**, *9* (5), 314–320.
- (55) Liu, T.; Sen, P.; Kim, C. J. Characterization of Nontoxic Liquid-Metal Alloy Galinstan for Applications in Microdevices. *Journal of Microelectromechanical Systems* **2012**, *21* (2), 443–450. https://doi.org/10.1109/JMEMS.2011.2174421.
- (56) Kim, D.; Thissen, P.; Viner, G.; Lee, D. W.; Choi, W.; Chabal, Y. J.; Lee, J. B. Recovery of Nonwetting Characteristics by Surface Modification of Gallium-Based Liquid Metal Droplets Using Hydrochloric Acid Vapor. ACS Appl Mater Interfaces 2013, 5 (1), 179–185. https://doi.org/10.1021/am302357t.
- (57) Joshipura, I. D.; Persson, K. A.; Truong, V. K.; Oh, J.-H.; Kong, M.; Vong, M. H.; Ni, C.; Alsafatwi, M.; Parekh, D. P.; Zhao, H. Are Contact Angle Measurements Useful for Oxide-Coated Liquid Metals? *Langmuir* **2021**, *37* (37), 10914–10923.
- (58) Ma, J.; Bharambe, V. T.; Persson, K. A.; Bachmann, A. L.; Joshipura, I. D.; Kim, J.; Oh, K. H.; Patrick, J. F.; Adams, J. J.; Dickey, M. D. Metallophobic Coatings to Enable Shape Reconfigurable Liquid Metal inside 3D Printed Plastics. ACS Appl Mater Interfaces 2020, 13 (11), 12709–12718.
- (59) Liu, S.; Sun, X.; Kemme, N.; Damle, V. G. G.; Schott, C.; Herrmann, M.; Rykaczewski, K. Can Liquid Metal Flow in Microchannels Made of Its Own Oxide Skin? *Microfluid Nanofluidics* **2016**, *20* (1), 1–6.
- (60) Wübben, T.; Stanzick, H.; Banhart, J.; Odenbach, S. Stability of Metallic Foams Studied under Microgravity. *Journal of Physics: Condensed Matter* **2002**, *15* (1), S427.
- (61) Yang, C. C.; Nakae, H. The Effects of Viscosity and Cooling Conditions on the Foamability of Aluminum Alloy. *J Mater Process Technol* **2003**, *141* (2), 202–206.
- (62) Yang, C. C.; Nakae, H. Foaming Characteristics Control during Production of Aluminum Alloy Foam. *J Alloys Compd* **2000**, *313* (1–2), 188–191.
- (63) Alargova, R. G.; Warhadpande, D. S.; Paunov, V. N.; Velev, O. D. Foam Superstabilization by Polymer Microrods. *Langmuir* **2004**, *20* (24), 10371–10374.
- (64) ASTM. Standard Test Method for Thermal Transmission Properties of Thermally Conductive Electrically Insulating Materials. *ASTM International* **2006**, *D5470*.
- (65) Thompson, D. R.; Rao, S. R.; Cola, B. A. A Stepped-Bar Apparatus for Thermal Resistance Measurements. *J Electron Packag* **2013**, *135* (4), 41002.

- (66) Uppal, A.; Kong, W.; Rana, A.; Wang, R. Y.; Rykaczewski, K. Enhancing Thermal Transport in Silicone Composites via Bridging Liquid Metal Fillers with Reactive Metal Co-Fillers and Matrix Viscosity Tuning. *ACS Appl Mater Interfaces* **2021**, *13* (36), 43348–43355.
- (67) Ralphs, M.; Kong, W.; Wang, R. Y.; Rykaczewski, K. Thermal Conductivity Enhancement of Soft Polymer Composites through Magnetically-Induced Percolation and Particle-Particle Contact Engineering. *Adv Mater Interfaces* **2019**, *1801857* (6), 6. https://doi.org/10.1002/admi.201801857.

TOC

